PERGAMON

Computers and Structures 70 (1999) 229–241

Computers & Structures

Adaptive computation of impact force under low velocity impact

P. Mahajan [a,*], A. Dutta [b]

[a] *Indian Institute of Technology Delhi, Hauz Khas, New Delhi 110016, India*
[b] *R.E.C. Silchar, 788010, India*

Received 18 January 1997; accepted 15 February 1998

Abstract

A simple and computationally efficient adaptive finite element analysis strategy has been adopted for accurate and reliable evaluation of contact force under low velocity impact. Contact of a spherical and cylindrical impactor on isotopic plates is considered. Adaptive mesh refinement enables the finite element mesh to be obtained automatically and the refined meshes influence the calculated contact force. Velocity and mass of impactor has some influence on discretization error as the discretization error changes with the change of these parameters.

Keywords: Finite element analysis; Contact force; Low velocity impact

1. Introduction

Adaptive finite element analysis is a subject of great importance if confidence in results of engineering application is needed. Without assessment of the reliability of the results it is hardly reasonable to use numerical methods like the finite element method in contact impact problems of plate and many other sensitive areas. Designing of an appropriate finite element mesh for contact impact problems is not an easy task and it could be very erroneous if made on the basis of intuition alone. Hence, a mesh obtained adaptively with densities varying according to the requirement of the problem is always a welcome choice.

At the present state of knowledge, the work recorded on adaptive finite element analysis under dynamic loads is limited. Wilson and Joo [1] have arrived at the final mesh using Ritz vector as the basis of transformation. In their investigation, the authors have made use of modal participation and amplification factors and obtained error estimates based on Babuska's criterion using amplified Ritz modes. Cook and Avrashi [2] have discussed the procedure for estimating the discretization error of the finite element modelling as applied to the calculation of natural frequency of vibrations. Meshes are obtained corresponding to each mode. Wiberg and Li [3] have proposed a post-processed type of *posteriori* estimates in space and also in time when direct integration is used for dynamic response evaluation. It updates the spatial mesh and time step so that the discretization errors are controlled. Dutta and Ramakrishnan [4] proposed a measure for discretization which is a logical extension of Zienkiewicz and Zhu [5] error criterion by involving time integration to consider the variation of response with time. Using this error measure, an adaptive mesh refinement strategy is proposed which yields good control over the discretization errors in transient dynamic analysis. For a chosen number of basis modes satisfying the modal cut-off criteria, an optimal mesh is attained iteratively wherein meshes are refined on the basis of error indicators so that the discretization errors are within the prescribed limit, when the modal superposition method is used. This strategy has been effectively carried out by Dutta and Ramakrishnan for

* Correspondence author.

0045-7949/99/$ - see front matter
PII: S0045-7949(98)00075-3

plate and shell bending problems under transient dynamic loads [6].

In this paper, we have adopted the adaptive strategy given by Dutta and Ramakrishnan [4] for the accurate evaluation of contact force under low velocity impact. The contact problem of a spherical impactor on an isotropic plate is solved using a Hertzian contact law. Effects of impact velocity and mass of impactor on space domain discretization errors are investigated. Similarly, adaptive analysis of contact problems between a cylindrical impactor with a barrelled end and an isotropic plate is also studied. Appropriate contact law is assumed for the force–deformation relationship. The well known degenerate shell element by Ahmad et al. [7] is used for evaluation of response under dynamic loads. The present study can be easily extended to composite plates subjected to transverse low velocity impact, which has been a major issue due to composite material's weak impact-resistance properties.

2. Finite element equation

The finite element model used here is an eight-noded degenerate shell element [7]. Five degrees of freedom are specified at each nodal point corresponding to its three displacements and the two rotations of the normal at the node. The definition of independent rotational and displacement degrees of freedom permits transverse shear deformation to be taken into account, since the rotations are not tied to the slope of the mid-surface. By neglecting damping, the governing equation of motion can be written as

$$\mathbf{M}\ddot{\mathbf{z}} + \mathbf{K}\mathbf{z} = \mathbf{q}(t). \tag{1}$$

At time $t + \Delta t$, Eq. (1) is written as

$$\mathbf{M}\ddot{\mathbf{z}}_{t+\Delta t} + \mathbf{K}\mathbf{z}_{t+\Delta t} = \mathbf{q}(t + \Delta t), \tag{2}$$

where $\mathbf{M}$ is the mass matrix, $\mathbf{K}$ is the linear elastic stiffness matrix and $\mathbf{q}$ is the force vector. In the numerical integration of the stiffness matrix $\mathbf{K}$, a selective integration method is employed. The 3×3 Gaussian rule is used to compute the stiffness coefficients for the in-plane and bending deformation and the reduced 2×2 Gaussian rule to compute the stiffness coefficients for the transverse shear deformation. In the thickness direction, two Gauss points are sufficient to capture the bending behaviour. The Newmark method is employed to obtain the solution to this equation. Accordingly the velocity and acceleration vectors at time $t + \Delta t$ are written as

$$\dot{\mathbf{z}}_{(t+\Delta t)} = \dot{\mathbf{z}}_{(t)} + \Delta t\{(1-\gamma)\ddot{\mathbf{z}}_{(t)} + \gamma\ddot{\mathbf{z}}_{(t+\Delta t)}\}, \tag{3}$$

$$\ddot{\mathbf{z}}_{(t+\Delta t)} = \frac{1}{\beta\Delta t^2}(\mathbf{z}_{(t+\Delta t)} - \mathbf{z}_{(t)}) - \frac{1}{\beta\Delta t}\dot{\mathbf{z}}_{(t)} - \left(\frac{1}{2\beta} - 1\right)\ddot{\mathbf{z}}_{(t)}. \tag{4}$$

The parameters β and γ are constants whose values depend on the finite difference scheme used in the calculations. Here we used the constant-average acceleration method, which is implicit and unconditionally stable. For this method β and γ are 1/4 and 1/2, respectively. Substituting of Eq. (4) into Eq. (2), we obtain

$$\mathbf{K}^*\mathbf{z}_{t+\Delta t} = \mathbf{q}^*(t + \Delta t), \tag{5}$$

where $\mathbf{K}^*$ is the effective stiffness matrix, and $\mathbf{q}^*(t + \Delta t)$ is the effective force vector. These parameters are defined as

$$\mathbf{K}^* = \frac{1}{\beta(\Delta t)^2}\mathbf{M} + \mathbf{K}, \tag{6}$$

$$\mathbf{q}^*(t + \Delta t) = \mathbf{h}(t) + \mathbf{q}(t + \Delta t), \tag{7}$$

where $\mathbf{h}(t)$ is the following vector

$$\mathbf{h}(t) = \mathbf{M}\left(\frac{1}{\beta\Delta t^2}\mathbf{z}_t + \frac{1}{\beta\Delta t}\dot{\mathbf{z}}_t + \frac{1-2\beta}{2\beta}\ddot{\mathbf{z}}_t\right). \tag{8}$$

3. Error estimation and adaptive analysis

Error estimation is carried out based on the strategy adopted by Dutta and Ramakrishnan [4]. In this method, error at each time step is calculated by comparing element level stresses obtained by finite element analysis and corresponding accurate stresses obtained by some post-processing technique. In this paper, we have used superconvergent patch recovery techniques [8] for obtaining accurate stresses. In the recovery process, it is assumed that the accurate nodal values $\bar{\sigma}^*$ belong to a polynomial expansion σ_e^* of the same complete order 'p' as that present in the basis function $\mathbf{N}$ and which is valid over an element patch surrounding the particular assembly node considered. Such a 'patch' represents a union of elements containing this vertex node (Fig. 1). This polynomial expansion will be used for each component of σ_e^* to give

$$\sigma_e^* = \mathbf{P}\mathbf{a}, \tag{9}$$

where $\mathbf{P}$ contains the appropriate polynomial terms and $\mathbf{a}$ is a set of unknown parameters. For an eight-noded quadrilateral element

$$\mathbf{P} = [1, x, y, x^2, xy, y^2, x^2y, xy^2], \tag{10}$$

and

$$\mathbf{a} = [a_1, a_2, a_3, a_4, a_5, a_6, a_7, a_8]^{\mathrm{T}}. \tag{11}$$

The determination of the unknown parameters $\mathbf{a}$ in Eq. (9) is best made by ensuring a least squares fit of this to the set of superconvergent points existing in the patch considered. To do this we minimize

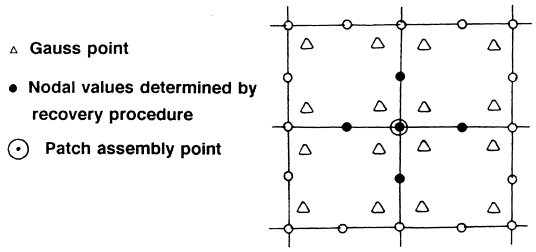

Fig. 1. Computation of superconvergent nodal values: △ Gauss point; • nodal values determined by recovery procedure; ⊙ patch assembly point.

$$F(\mathbf{a}) = \sum_{i=1}^{n} (\sigma_e(x_i, y_i) - \sigma_e^*(x_i, y_i))^2 = \sum_{i=1}^{n} (\sigma_e(x_i, y_i) - \mathbf{P}(x_i, y_i)\mathbf{a})^2, \quad (12)$$

where (x_i, y_i) are the co-ordinates of a group of sampling points, $n = mk$ is the total number of sampling points and k is the number of the sampling points on each element $m_i (m_i = 1,2,\ldots m)$ of the element patch. The minimization condition of $F(\mathbf{a})$ implies that $\mathbf{a}$ satisfies

$$\sum_{i=1}^{n} \mathbf{P}^{\mathrm{T}}(x_i, y_i)\mathbf{P}(x_i, y_i)\mathbf{a} = \sum_{i=1}^{n} \mathbf{P}^{\mathrm{T}}(x_i, y_i)\sigma_e(x_i, y_i). \quad (13)$$

This can be solved in matrix form as

$$\mathbf{a} = \mathbf{A}^{-1}\mathbf{b}, \quad (14)$$

where

$$\mathbf{A} = \sum_{i=1}^{n} \mathbf{P}^{\mathrm{T}}(x_i, y_i)\mathbf{P}(x_i, y_i)$$

$$\text{and } \mathbf{b} = \sum_{i=1}^{n} \mathbf{P}^{\mathrm{T}}(x_i, y_i)\sigma_e(x_i, y_i). \quad (15)$$

The unknown vector $\mathbf{a}$ as determined for a particular patch assembly point is used to evaluate the nodal values $\bar{\sigma}^*$ of the patch assembly point and all other surrounding nodes in that patch by insertion of appropriate co-ordinates into the expression for σ_e^*. Such surrounding nodes have been marked • in Fig. 1.

The mathematical basis and details of the domain discretization error algorithm are described in ref. [4]. The complete procedure of discretization error measure is given below in algorithmic form Table 1.

Thus, starting with a coarse mesh, discretization errors at element level $\xi_i' (I = 1$, no. of elements) are determined using the algorithm described above for a reasonably fine value of 'Δt'. Mesh is then adaptively refined based on the ξ_i' values obtained and overall domain discretization error η and discretization error at element level ξ_i' are determined again. Iteration is carried out until the mesh is an optimal one for the prescribed discretization error limit $\bar{\eta}$ corresponding to the adopted time step size. An automatic quadrilateral mesh generator developed by Sinha and Ramakrishnan [9] has been utilized for adaptively designing the finite element meshes. The methodology adopted for the generation of these unstructured meshes are based on the ideas used in the advancing front techniques by Peraire and co-workers [10] and paving techniques by Blacker and Stephenson [11]. A new and more general formulation, which offers the advantages of encompassing a whole class of techniques within a single framework is utilised. It is rule driven, offering flexibility through the incorporated constraints with the possibility of adaptive modification. Starting from a domain discretized into a polygon having even number of sides, the average nodal spacing is specified over the domain as input and the whole domain is meshed by non-overlapping quadrilaterals.

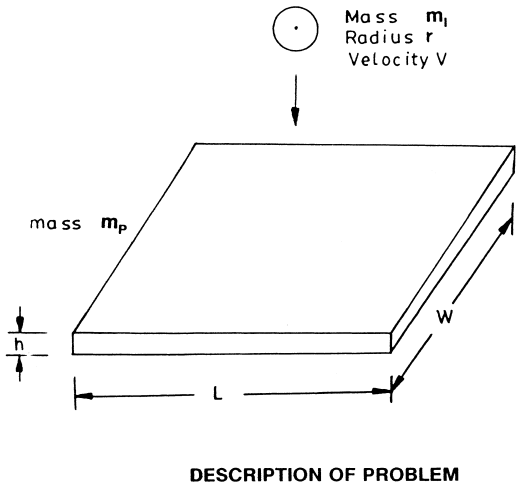

Fig. 2. Description of problem.

Table 1
Algorithm for domain discretization error

(1) Solve $\mathbf{M}\ddot{\mathbf{z}} + \mathbf{K}\mathbf{z} = \mathbf{q}(t)$

(1.1) Using Newmark method calculate dynamic response for $t = 0,\ T$

{

$$\mathbf{K}^{*}\mathbf{z}_{t+1} = \mathbf{q} * (t+1),$$

$$\ddot{\mathbf{z}}_{(t+1)} = \frac{1}{\beta\Delta t^{2}}(\mathbf{z}_{(t+1)} - \mathbf{z}_{(t)}) - \frac{1}{\beta\Delta t}\dot{\mathbf{z}}_{(t)} - \left(\frac{1}{2\beta} - 1\right)\ddot{\mathbf{z}}_{(t)},$$

$$\dot{\mathbf{z}}_{(t+1)} = \dot{\mathbf{z}}_{(t)} + \Delta t\{(1-\gamma)\ddot{\mathbf{z}}_{(t)} + \gamma\ddot{\mathbf{z}}_{(t+1)}\}.$$

(1.2) for $e = 1,\ n$ elements

{

Retrieve $\mathbf{z}_{\mathbf{e}_{(t)}}$ from $\mathbf{z}_{(t)}$

for $j = 1$, number of Gaussian point

{

calculate

$\sigma^{(j)}_{\mathbf{e}_{(t)}} = \mathbf{D}\mathbf{B}^{(j)}\mathbf{z}_{e_{(t)}}$,

calculate smooth stress $\sigma^{*(j)}_{\mathbf{e}_{(t)}}$

$$\mathbf{e}^{(j)}_{\sigma\mathbf{e}_{(t)}} = \sigma^{*(\mathrm{j})}_{\mathbf{e}_{(t)}} - \sigma_{\mathbf{e}_{(t)}},$$

$$||\mathbf{e}||_{\mathbf{e}_{(t)}} = \left[\int_{\Omega}\left(\mathbf{e}^{(j)}_{\sigma\mathbf{e}_{(t)}}\right)^{\mathrm{T}}\mathbf{D}_{\mathrm{e}}^{-1}\mathbf{e}^{(j)}_{\sigma\mathbf{e}_{(t)}}\,\mathrm{d}\Omega\right]^{1/2},\quad ||\bar{\mathbf{u}}||_{\mathbf{e}_{(t)}} = \left[\int_{\Omega}\left(\sigma^{(j)}_{\mathbf{e}_{(t)}}\right)^{\mathrm{T}}\mathbf{D}_{\mathrm{e}}^{-1}\sigma^{(j)}_{\mathbf{e}_{(t)}}\,\mathrm{d}\Omega\right]^{1/2},$$

}

for the whole structure

$$||\mathbf{e}||_{(t)} = \left[\sum ||\mathbf{e}||^{2}_{\mathbf{e}_{(t)}}\right]^{1/2},\quad ||\bar{\mathbf{u}}||_{(t)} = \left[\sum ||\bar{\mathbf{u}}||^{2}_{\mathbf{e}_{(t)}}\right]^{1/2}.$$

}

}

2. Overall domain discretization error

$$||\mathbf{e}||_{\mathrm{av}} = \frac{\int_{0}^{T}||\mathbf{e}||_{(t)}\,\mathrm{d}t}{T},$$

$$||\mathbf{u}||_{\mathrm{av}} = \frac{\int_{0}^{T}||\mathbf{u}||_{(t)}\,\mathrm{d}t}{T},$$

where

$$||\mathbf{u}||_{(t)} = \left[||\bar{\mathbf{u}}||^{2}_{(t)} + ||\mathbf{e}||^{2}_{(t)}\right]^{1/2},\quad \eta = \frac{||\mathbf{e}||_{\mathrm{av}}}{||\mathbf{u}||_{\mathrm{av}}} \times 100\%.$$

3. Discretization error at element level

For $l = 1,\ n$ elements

{

where

$$\xi_{i} = \frac{||\mathbf{e}||_{i_{(t)}}}{\bar{\mathbf{e}}_{m}},$$

$$\bar{\mathbf{e}}_{m} = \bar{\eta}\left[\frac{||\bar{\mathbf{u}}||^{2}_{(t)} + ||\mathbf{e}||^{2}_{(t)}}{n}\right]^{1/2},$$

$$\xi'_{i} = \frac{\int_{0}^{mT}\xi_{i}\,\mathrm{d}t}{T}.$$

If $\eta \leq \bar{\eta}$ and

If $\xi'_{i} < 1$ for $l = 1,\ n$ STOP

Else

$$h_{i_{\mathrm{new}}} = \frac{h_{i_{\mathrm{old}}}}{(\xi'_{i})^{\phi}},$$

where $\phi = 1/\mathrm{p}$ for no singularity (p is the order of polynomial used in the finite element formulation), and $\phi = 1/\lambda$ for elements close to singularity (λ is the strength of singularity)

Endif}

Go to step 1

4. Indentation law

When a plate is impacted by a mass, the magnitude of contact force which results because of the impact is not known a priori. This contact force needs to be calculated before the plate motion is analysed using Eq. (5). The evaluation of contact force depends on a contact law which relates the contact force with the indentation.

4.1. Contact of a sphere with a plate

The projectile is modelled as a spherical elastic body as shown in Fig. 2. During loading and unloading, the contact force distribution was determined using the Hertzian contact law. Thus, the contact force F can be related to the indentation depth α, the distance between the centre of the projectile's nose and mid-surface of the plate by the expression

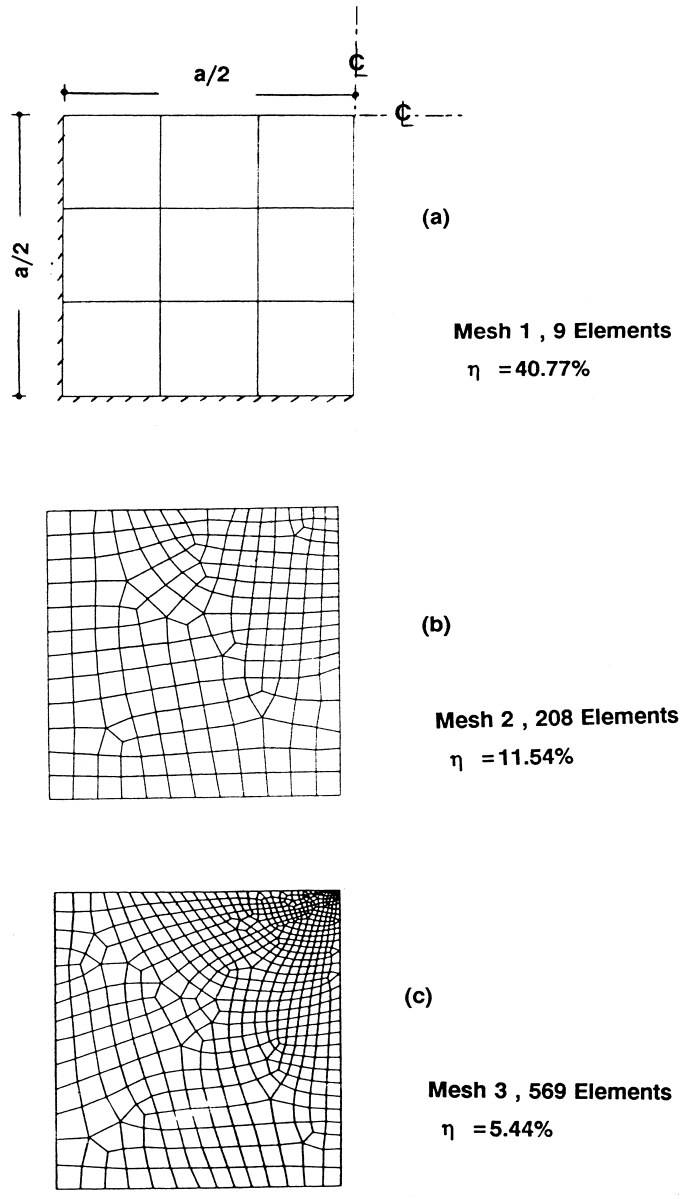

Fig. 3. Symmetric quadrant of clamped square plate ($a/t = 25$) subjected to impact by a sphere at the centre of the plate.

$$F = \mathbf{K}\alpha^{1.5}, \tag{16}$$

where $\mathbf{K}$ is the modified constant of the Hertz contact theory proposed by Sun et al. [12]

$$\mathbf{K} = \frac{4}{3}\sqrt{r}\frac{1}{[(1-v_s^2)/E_I + 1/E_T]}, \tag{17}$$

where r, v_s, and E_I are the local radius, the Poisson's ratio and the Young's modulus of the impactor, respectively. E_T is the Young's modulus of the target.

4.2. Solution procedure

The unknowns in Eq. (5) are the displacement vector $\mathbf{z}_{t+\Delta t}$ and the force vector $\mathbf{q}(t+\Delta t)$ since the displacement, velocity and acceleration at time 't' are known at every point inside the plate. To determine these two unknowns, an additional expression is needed, which is developed below following the procedure mentioned in ref. [13].

In the absence of body forces, for a plate initially at rest, the only concentrated load is the contact force caused by the impactor. We define a scalar force 'f' which is a point force acting perpendicular to the plate at the contact point and has a magnitude equal to the contact force. The contact vector $\mathbf{q}$ is then written as

$$\mathbf{q} = f\mathbf{u}, \tag{18}$$

$\mathbf{u}$ is a unit vector which is equal to -1 in the direction of the contact force at the point of contact and zero elsewhere. The displacement vector $\mathbf{z}$ is expressed as the sum of the displacements due to the force $\mathbf{h}$ and the contact force $\mathbf{q}$

$$\mathbf{z}_{t+\Delta t} = \mathbf{z}^{\mathbf{h}}_{t+\Delta t} + \mathbf{z}^{\mathbf{q}}_{t+\Delta t}. \tag{19}$$

Thus we can write

$$\mathbf{K}^*\left(\mathbf{z}^{\mathbf{h}}_{t+\Delta t} + \mathbf{z}^{\mathbf{q}}_{t+\Delta t}\right) = \mathbf{h}(t) + \mathbf{q}(t+\Delta t). \tag{20}$$

From Eq. (20) we have

$$\mathbf{K}^*\mathbf{z}^{\mathbf{h}}_{t+\Delta t} = \mathbf{h}(t), \tag{21}$$

$$\mathbf{K}^*\mathbf{z}^{\mathbf{q}}_{\mathbf{t+\Delta t}} = \mathbf{q}(\mathbf{t}+\mathbf{\Delta t}). \tag{22}$$

The solution of Eqs. (21) and (22) now proceeds in two steps. First, the forces $\mathbf{h}$ and the displacements $\mathbf{z}^{\mathbf{h}}$ are calculated from Eqs. (8) and (21), respectively. Second, the contact force vector $\mathbf{q}$ and the displacement $\mathbf{z}^{\mathbf{q}}$ are calculated as follows. At time $t+\Delta t$, Eq. (18) is written as

$$\mathbf{q}(t+\Delta t) = f(t+\Delta t)\mathbf{u}. \tag{23}$$

Eqs. (22) and (23) yield

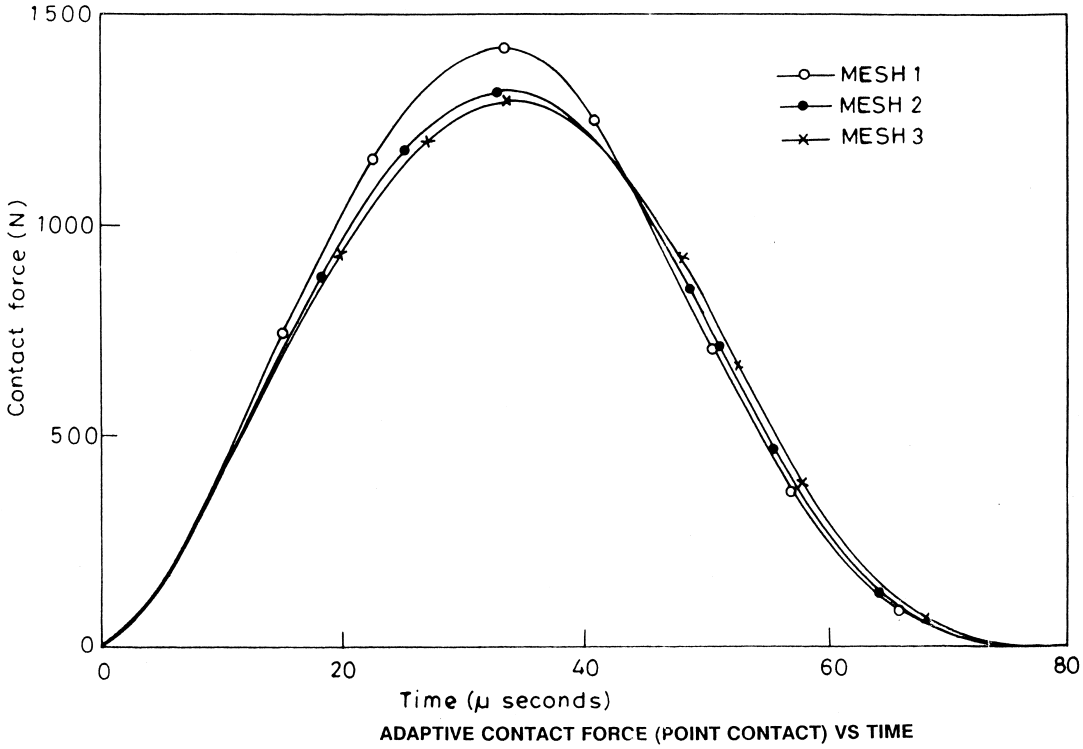

Fig. 4. Adaptive contact force (point contact) vs time.

$$\mathbf{K}^{*}\mathbf{z}^{\mathbf{q}}_{t+\Delta t} = f(t+\Delta t)\mathbf{u}. \tag{24}$$

For a unit contact force ($f(t+\Delta t)=1$), Eq. (24) becomes

$$\mathbf{K}^{*}\mathbf{z}^{\mathbf{u}}_{t+\Delta t} = \mathbf{u}, \tag{25}$$

where $\mathbf{z}^{\mathbf{u}}{}_{t+\Delta t}$ is the displacement caused by the unit contact force. From Eqs. (24) and (25), it is seen that $\mathbf{z}^{\mathbf{q}}{}_{t+\Delta t}$ and $\mathbf{z}^{\mathbf{u}}{}_{t+\Delta t}$ are related by

$$\mathbf{z}^{\mathbf{q}}_{t+\Delta t} = f(t+\Delta t)\mathbf{z}^{\mathbf{u}}_{t+\Delta t}. \tag{26}$$

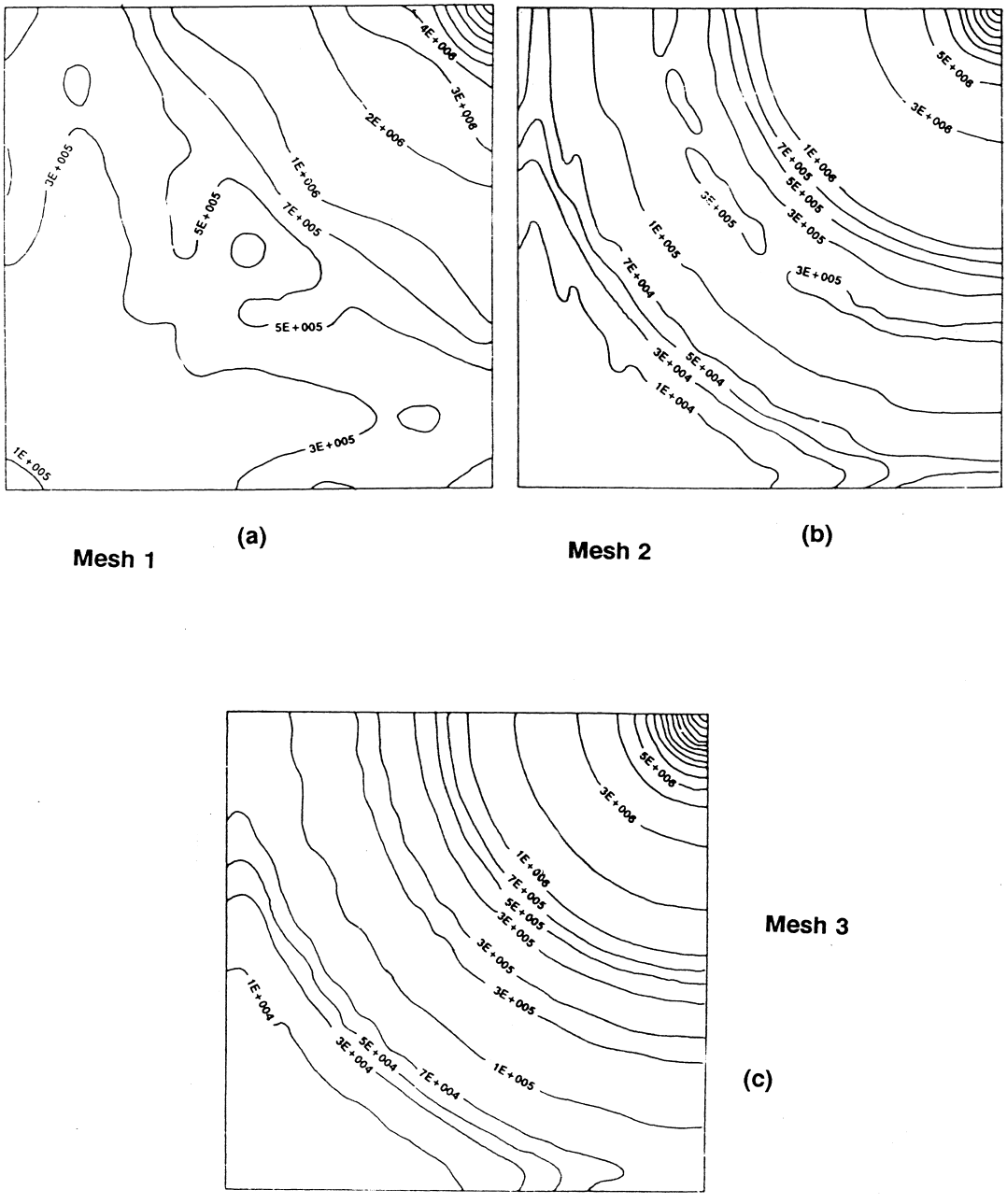

Fig. 5. Effective stress (N/m^2) contours of target plate impacted by spherical impactor.

Eqs. (19) and (26) give

$$\mathbf{z}_{t+\Delta t} = \mathbf{z}^{\mathbf{h}}_{t+\Delta t} + f(t+\Delta t)\mathbf{z}^{\mathbf{u}}_{t+\Delta t}. \tag{27}$$

In Eq. (27), the unknowns are the displacement vector $\mathbf{z}$ and the scalar force 'f' at time $t+\Delta t$. In order to find these two unknowns, another expression for the contact force is required. The expression for contact force during the loading and unloading processes was given in Eq. (16) earlier.

The indentation depth α varies with time and at time $t+\Delta t$ this depth is

$$\alpha^{t+\Delta t} = \delta^s_{t+\Delta t} - \delta^c_{t+\Delta t}, \tag{28}$$

$\delta^c{}_{t+\Delta t}$ is the displacement of the centre of the mid-surface of the plate in the direction of the impact. With the use of Eq. (27), δ^c can be expressed as

$$\delta^c_{t+\Delta t} = \delta^{ch}_{t+\Delta t} + f(t+\Delta t)\delta^{cu}_{t+\Delta t}, \tag{29}$$

$\delta^s{}_{t+\Delta t}$ is the position of the centre point of the impactor. At time $t+\Delta t$, the magnitude of $\delta^s{}_{t+\Delta t}$ is determined by Newton's second law

$$\delta^s_{t+\Delta t} = \int_0^{t+\Delta t}\int_0^{t+\Delta t} \frac{f}{m}\,\mathrm{d}t\,\mathrm{d}t, \tag{30}$$

where 'f' is the time varying force and 'm' is the impactor mass.

By combining Eqs. (28) and (30), we obtain the following expressions for the contact force:

During loading and unloading

$$f(t+\Delta t) = \mathbf{K}\left(\int_0^{t+\Delta t}\int_0^{t+\Delta t} \frac{f}{m}\,\mathrm{d}t\,\mathrm{d}t - \delta^{ch}_{t+\Delta t} - f(t+\Delta t)\delta^{cu}_{t+\Delta t}\right)^{1.5}. \tag{31}$$

The contact force 'f' is calculated by Eq. (31) (during loading and unloading) by Newton–Raphson method.

4.3. Numerical example

an isotropic square steel plate 20 cm long, 20 cm wide, and 8 mm thick rigidly fixed on its four edges. The plate is subjected to an impact induced by a steel ball of 2 cm diameter to its centre with a velocity of 100 cm/s.

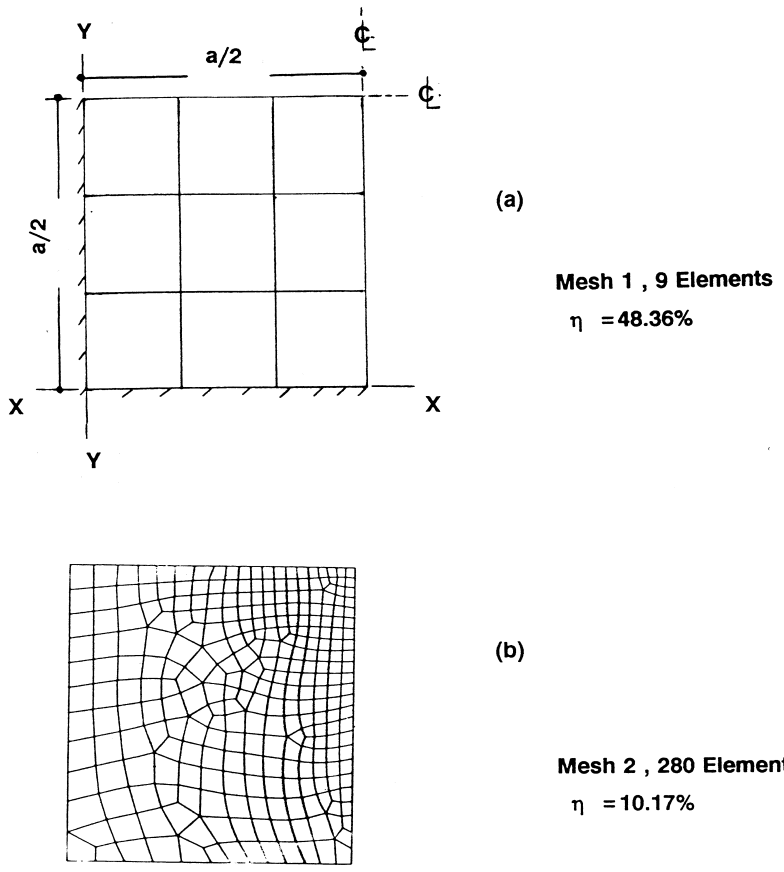

Fig. 6. Symmetric quadrant of clamped square plate ($a/t = 25$) subjected to impact by a cylinder along central line (parallel to XX) of the plate.

A quadrant of the square plate is considered for the analysis and the adaptive analysis is carried out for a prescribed domain discretization error limit $\bar{\eta} = 5\%$. Three analyses are needed to bring the overall domain discretization error η near to 5%. The initial mesh [Fig. 3(a)] has nine elements and the overall domain discretization error $\eta = 40.77\%$. The mesh is then refined based on the local error values and the new mesh [Fig. 3(b)] has 208 elements with overall domain discretization error $\eta = 11.54\%$. Refinement is again carried out and the final mesh [Fig. 3(c)] with 569 elements has $\eta = 5.44\%$. In the present paper adaptivity in spatial domain has been considered only and hence time step is not adjusted adaptively. But the error in time domain has been controlled by choosing a sufficiently fine time step of the order of 10^{-4} and it has been observed that by further reducing to 5×10^{-5}, the variation in the contact force is less than 0.5%. Fig. 4 shows the plot of contact force vs time corresponding to each of these meshes and it is clear from the Fig. 4 that the finite element mesh influences the value of the contact force so calculated. Maximum value of the contact force reduces from 1417.5 N corresponding to mesh 1 [Fig. 3(a)] to 1291.1 N corresponding to the final mesh [Fig. 3(c)]. Maximum plate displacement at the point of contact increases from 8.38×10^{-4} to 8.85×10^{-4} cm. The effective stress contours of target plate impacted by spherical impactor at 34 micro seconds (time corresponding to the peak contact force) as shown in Fig. 5 indicates that stress distribution changes with the mesh refinement. The effective stress increases near the point of contact and reduces towards the opposite corner with mesh refinement. The effective stress increased from 1.11×10^7 N/m^2 corresponding to mesh 1 [Fig. 3(a)] to 2.27 N/m^2 corresponding to mesh 3 [Fig. 3(c)]. Contact period is also observed to increase by a few micro-seconds as finer and finer meshes are used. The solutions compare well with the series solution of Karas and the finite element solution as presented in ref. [13].

4.4. Contact of a cylinder with a plate

A Hertzian distribution of pressure is assumed to act on the plate which is uniform along the length of the barrelled cylinder. In order to reduce the stress concentration at the ends, the axial profile of the cylinder should be slightly barrelled. The displacement at the centre of the contact [14] is

$$\delta(0,0) = \frac{f}{\pi l E^*}\{1.886 + \ln(l/a)\}, \tag{32}$$

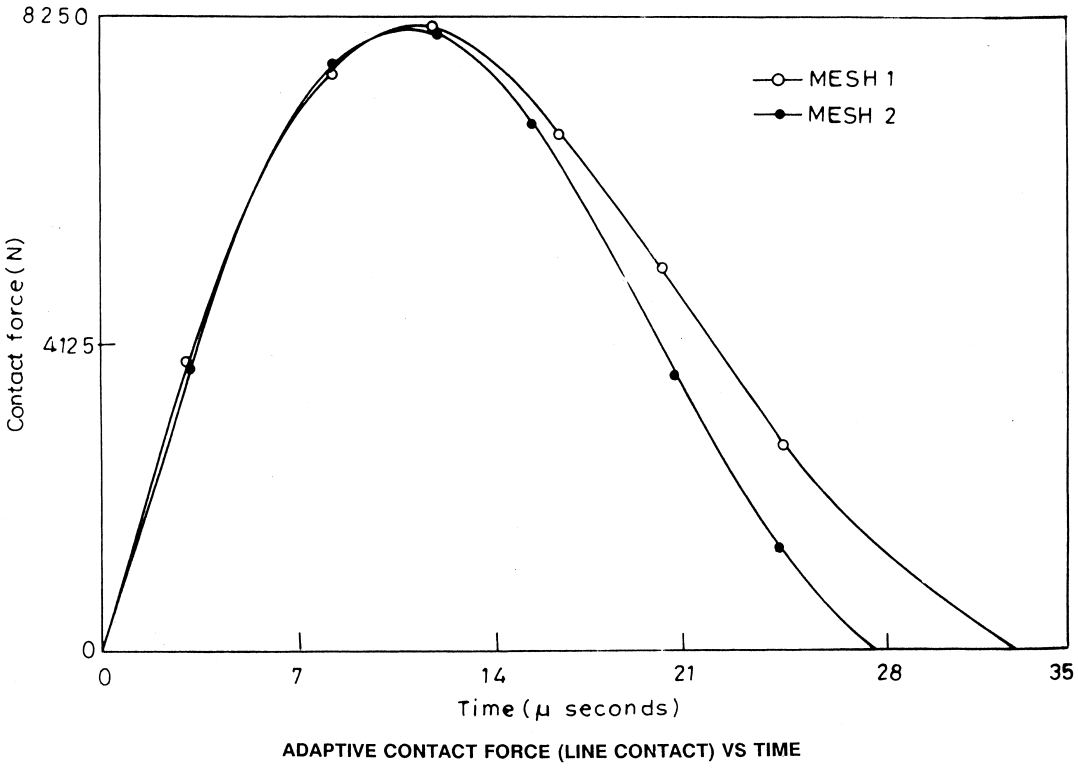

Fig. 7. Adaptive contact force (line contact) vs time.

where 'f' is the total contact force, '$2\,l$' is the length of the cylinder in contact, and

$$a=\sqrt{\frac{4fr}{\pi E^*}} \quad \text{and} \quad \frac{1}{E^*}=\frac{1-v_1^2}{E_1}+\frac{1-v_2^2}{E_2},$$

'r' is the radius of the cylinder, E_1 and E_2 are Young's modulus of impactor and target respectively and v_1 and v_2 are Poisson's ratio of impactor and target, respectively. Eq. (32) is considered as the relationship between indentation depth and contact force for both

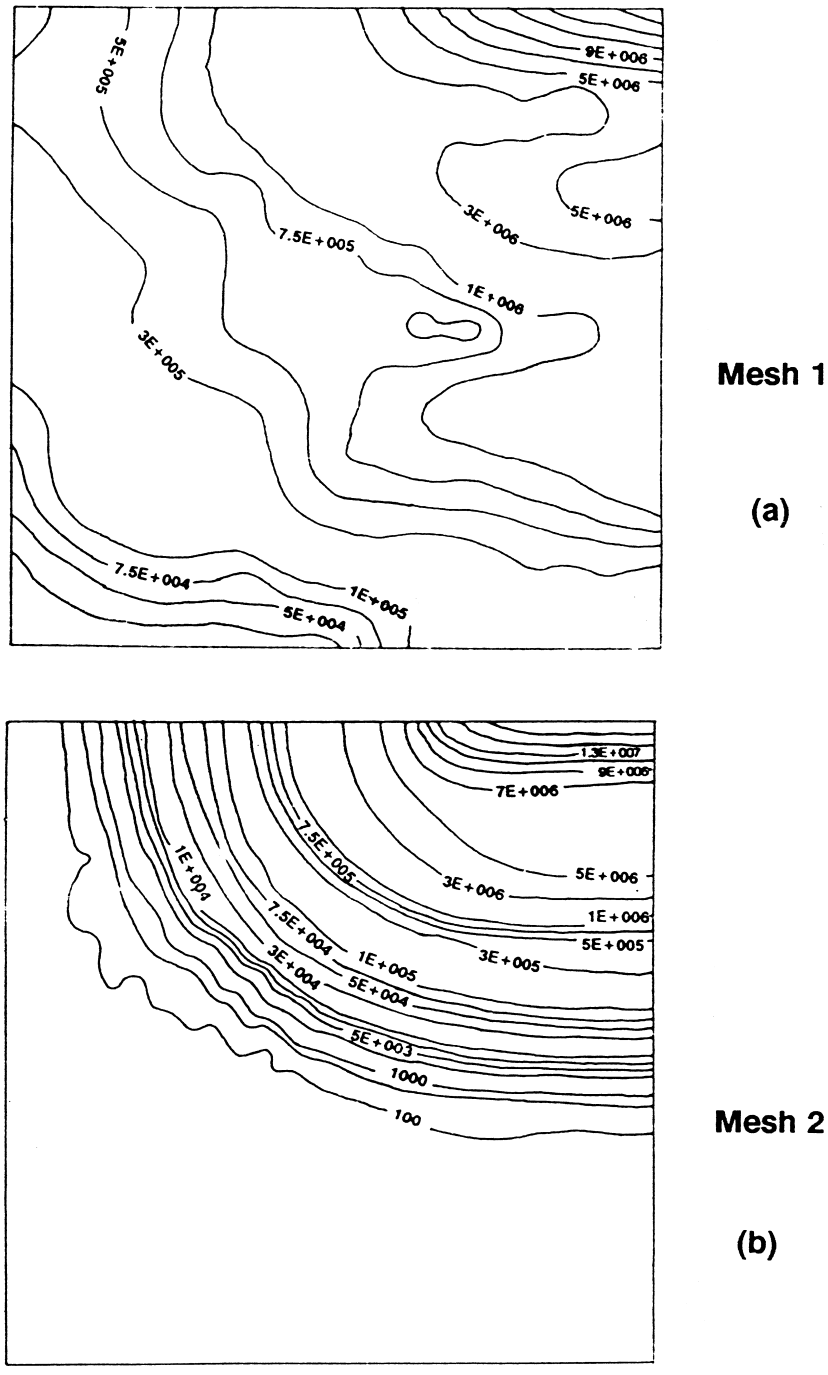

Fig. 8. Effective stress (N/m^2) contours of target plate impacted by cylindrical impactor.

Table 2
Discretization error for varying impactor velocities with a constant m_I/m_P ratio

Mesh	Impactor velocity (cm/s)	Domain discretization error η
Fig. 3(a)	100	40.73%
Fig. 3(a)	200	42.39%
Fig. 3(a)	500	44.24%

loading and unloading. The same solution procedure as mentioned earlier is followed here as well and leads to the expression for contact force during loading and unloading as

$$f(t+\Delta t) = \frac{\pi l E^*}{1.886 + \ln(l/a)} \times \left(\int_0^{t+\Delta t} \int_0^{t+\Delta t} \frac{f}{m} \, \mathrm{d}t \, \mathrm{d}t - \delta^{ch}_{t+\Delta t} - f(t+\Delta t)\delta^{cu}_{t+\Delta t} \right)^{1.5} \quad (33)$$

4.5. Numerical example

an isotropic square steel plate 20 cm long, 20 cm wide, and 8 mm thick rigidly fixed on its four edges. The plate is subjected to an impact induced by a steel cylinder of 2 cm diameter and 6.6667 cm length to its centre with a velocity of 100 cm/s.

A quadrant of the square plate is considered for the analysis and the adaptive analysis is carried out for a prescribed domain discretization error limit $\bar{\eta} = 10\%$. Two analyses are needed to bring the overall domain discretization error η near to 10%. The initial mesh [Fig. 6(a)] has nine elements and the overall domain discretization error $\eta = 48.36\%$. The mesh is then refined based on the local error values and the new mesh [Fig. 6(b)] has 280 elements with overall domain discretization error $\eta = 10.17\%$. Fig. 7 shows the plot of contact force vs time corresponding to each of these meshes indicating that the finite element mesh influences the value of the computed contact force. In this example, the difference in the value of maximum contact force corresponding to the coarse and fine mesh is marginal; but the contact durations are quite different. The contours (Fig. 8) showing von Mises stress distribution of a target plate impacted by a cylinder indicate that the stress profile changes substantially as the finite element mesh changes. The effective stress at the point of contact changes from 1.74×10^7 N/m^2 corresponding to mesh 1 [Fig. 6(a)] to 1.9×10^7 N/m^2 corresponding to mesh 2 [Fig. 6(b)]. The contact duration for cylindrical impactor problems are smaller compared to that of spherical impactor problems.

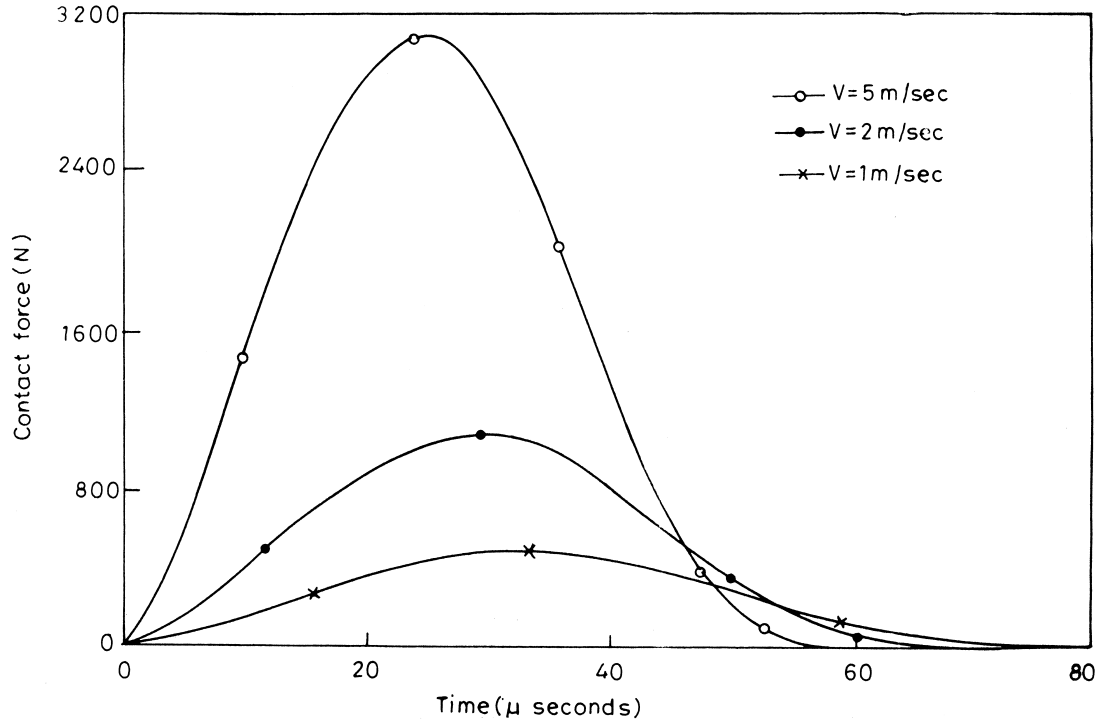

Fig. 9. Contact force (point contact) vs time for different impact velocity but fixed m_I/m_P.

Table 3
Discretization error for varying m_I/m_P ratios with a constant impactor velocity

Mesh	Ratio of impactor mass to mass of the plate (m_I/m_P)	Domain discretization error η
Fig. 3(a)	0.013	40.73%
Fig. 3(a)	0.037	35.38%
Fig. 3(a)	0.041	34.26%

5. Influence of impactor velocity and mass on space discretization error

In ref. [15], a study is conducted on composite laminates subjected to low velocity impact to ascertain the dependence of contact period and contact force on parameters like velocity of impactor and mass ratio of impactor to target plate. It is observed that the duration and the shape of the contact force history are not dependent on the velocity but on the mass ratio. If the mass ratio is less than one, the number of contacts between the impactor and laminates occur more than once; but if the ratio is one or more, the contact occurs only once. In the same line, a study is conducted to assess the influence of impactor velocity and impactor mass on domain discretization error. The impact of an aluminium ball on isotropic aluminium plate is considered. The geometrical data are the same as the point contact problem described earlier. The mesh in Fig. 3(a) is considered for the study. When the velocity of the impactor is varied keeping the mass of the impactor unchanged, it is observed that the domain discretization error slowly increases (Table 2). Hence, mesh refinement requirement also increases when velocity of the impactor is increased. Fig. 9 shows the plot of contact force vs time for different impactor velocities with a constant ratio of mass of impactor to mass of plate (m_I/m_P). Contact force increases with the increase in impactor velocity; but contact period decreases slightly.

The impact of spherical mass on an isotropic plate with a constant impactor velocity but with varying m_I/m_P is considered. The target is an aluminium plate; but the impactor material is varying. Error estimation for three different cases of m_I/m_P shows that the discretization error η decreases with the increase in the ratio of m_I/m_P (Table 3) and hence coarser and coarser meshes would be required. Fig. 10 shows the plot of contact force vs time for different m_I/m_P ratios with a constant impactor velocity. Both contact force and contact period increase with the increase in the ratio of m_I/m_P.

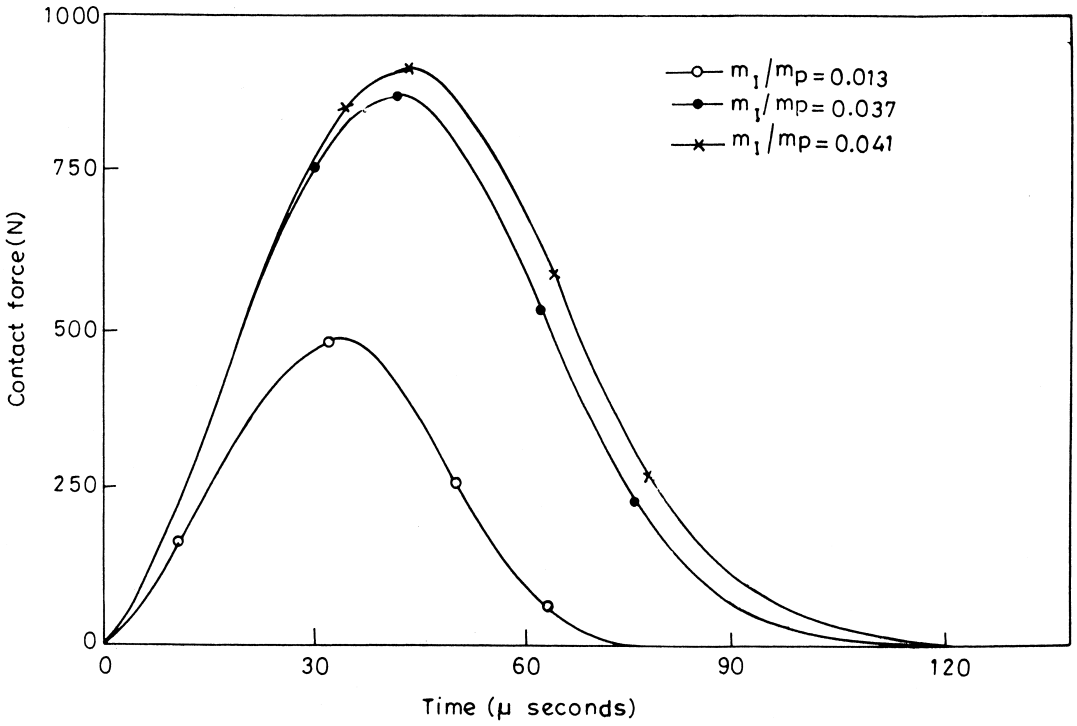

Fig. 10. Contact force (point contact) vs time for constant impact velocity but different m_I/m_P.

6. Conclusion

A discretization error measure based on time integrated Z–Z type of error estimate is effectively used. For a prescribed limit of $\bar{\eta}$, the optimal mesh is obtained iteratively. The computed contact forces change with the change in finite element mesh, where mesh is refined nearer the point of application of the contact force as the stress gradient will be high there. Discretization error is effected by the parameter like impactor velocity and ratio of mass of impactor to mass of plate.

References

[1] Joo KJ, Wilson EL. An adaptive finite element technique for structural dynamic analysis. Comput Struct 1988;30(6):1319–39.

[2] Cook RD, Avrashi J. Error estimation and adaptive meshing for vibration problems. Comput Struct 1992;44(3):619–26.

[3] Wiberg NE, Li XD. A post-processed error estimate and an adaptive procedure for the semidiscrete finite element method in dynamic analysis. Int J Numer Meth Engng 1994;37:3585–603.

[4] Dutta A, Ramakrishnan CV. Error estimation in finite element transient dynamic analysis using modal superposition. Engng Comput 1997;14:135–58.

[5] Zienkiewicz OC, Zhu JZ. A simple error estimator and adaptive procedure for practical engineering analysis. Int J Numer Meth Engng 1987;24:337–57.

[6] Dutta A, Ramakrishnan CV. in press. Adaptive finite element analysis of structures under transient dynamic loading using modal superposition. Finite Elements Anal. Design.

[7] Ahmad S, Irons BM, Zienkiewicz OC. Analysis of thick and thin shell structures by curved finite elements. Int J Numer Meth Engng 1970;2:419–51.

[8] Zienkiewicz OC, Zhu JZ. The superconvergent patch recovery and *a posteriori* error estimates. Part 1: the recovery technique. Int J Numer Meth Engng 1992;33:1331–64.

[9] Sinha A, Ramakrishnan CV. Growth methods and binary space partitioning for efficient finite element mesh generation, in press.

[10] Yang SH, Sun CT. Indentation law for composite laminates. NASA CR-165460, 1981.

[11] Peraire J, Vahdati M, Morgan K, Zienkiewicz OC. Adaptive remeshing for compressible flow computations. J Comp Phys 1987;72(2):449–66.

[12] Blacker TD, Stephenson MB. Paving: A new approach to automated quadrilateral mesh generation. Int J Numer Meth Engng 1991;32:811–47.

[13] Wu H-YT, Chang FK. Transient dynamic analysis of laminated composite plates subjected to transverse impact. Comput Struct 1989;31(3):453–66.

[14] Johnson KL. Contact Mechanics. Cambridge: Cambridge University, 1985.

[15] Choi IH, Hong CS. New approach for simple prediction of impact force history on composite laminates. AIAA J 1994;32(10):2067–72.